ORIGINAL PAPER

Red-emission carbon dots-quercetin systems as ratiometric fluorescent nanoprobes towards Zn^{2+} and adenosine triphosphate

Baogang Wang[1,2] · Zhu Liang[1] · Hui Tan[1] · Wenmeng Duan[1] · Mina Luo[1]

Abstract

Carbon dots (CDs) emitting red fluorescence (610 nm) were synthesized by solvent thermal treatment of p-phenylenediamine in toluene. Upon 440 nm excitation, quercetin (QCT) alone endowed slight effects on the red fluorescence of CDs. Once Zn^{2+} was further introduced, the QCT-Zn^{2+} complex was quickly formed. This complex absorbs excitation light and emits bright green fluorescence at 480 nm. The red fluorescence of CDs was greatly quenched owing to the inner-filter effect. The ratio of fluorescence intensity at 480 nm and 610 nm (I_{480}/I_{610}) gradually increases with increasing concentration (c) of Zn^{2+}. Al^{3+} exhibits the same phenomen like Zn^{2+}. Fluoride ions form a more stable complex with Al^{3+} than QCT-Al^{3+} complex but have a negligible effect on the QCT-Zn^{2+} complex. The possible interference of Al^{3+} on Zn^{2+} can thus be avoided by adding certain amount of F^-. The CD-QCT-F^- system was constructed as a ratio-metric fluorescent nanoprobe toward Zn^{2+} with determination range of 0.14–30 μM and limit of detection (LOD) of 0.14 μM. Due to the stronger affinity of adenosine triphosphate (ATP) to Zn^{2+} than QCT, the I_{480}/I_{610} value of CD-QCT-F^--Zn^{2+} system gradually decreases with increasing c_{ATP}. The ratiometric fluorescent nanoprobe toward ATP was established with detection ranges of 0.55–10 and 10–35 μM and a LOD of 0.55 μM. The above two probes enable the quantitative determination of Zn^{2+} and ATP in tap and lake water samples with satisfactory recoveries.

Keywords Fluorescent nanoprobe · Fluorescence quenching · Complex formation · ATP determination · Water samples

Introduction

Zn^{2+} plays critical roles in cell proliferation and differentiation, gene expression, signal transduction, and neurotransmission [1–3]. However, excess of Zn^{2+} can result in serious disorders such as diabetes, cerebral ischemia, epilepsy,

✉ Baogang Wang
bgwang@swpu.edu.cn

✉ Mina Luo
luo_mn@126.com

1 College of Chemistry and Chemical Engineering, Southwest Petroleum University, Chengdu 610500, People's Republic of China

2 Oil & Gas Field Applied Chemistry Key Laboratory of Sichuan Province, Chengdu 610500, People's Republic of China

Alzheimer's disease, cancer, and neural degeneration [4]. Adenosine triphosphate (ATP) plays important roles in many cellular events such as the active transport, enzymatic processes, and muscle contraction [5]. The abnormal levels of ATP were associated with diseases including angiocardiopathy, Parkinsonism, Alzheimer's, and cancer [6]. Thus, development of sensitive and selective methods for determining Zn^{2+} and ATP is of significant importance.

Among various determination methods for Zn^{2+} and ATP, fluorescent nanoprobes have attracted much attention because of their distinct merits such as high sensitivity, specific selectivity, real-time monitoring, and operational simplicity. Many fluorescent nanoprobes have builted by conventional fluorescent materials including organic dyes, semiconductor quantum dots, rare elements, and metal nanoclusters. The carbon dot (CD)-based fluorescent nanoprobes have attracted more attention due to their low cost, good water solubility, high photo stability, and favorable biocompatibility [7–10]. Despite some CD-based nanoprobes have been established

Scheme 1 Schematic illustration of **a** the preparation of CDs and **b** their subsequent application as the ratio-metric fluorescent probes towards Zn^{2+} and ATP with the aid of QCT
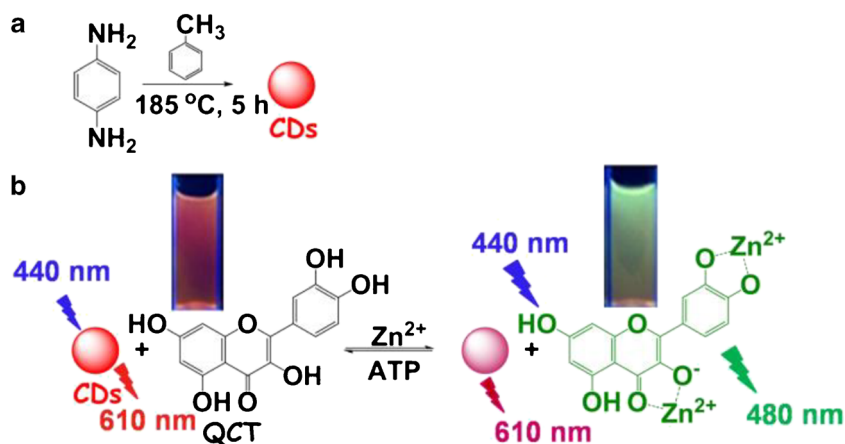
for Zn^{2+} determination [4, 11–20], several key issues need to be solve before their practical applications. First, some nanoprobes were constructed by the CDs covalently linked with organic molecules or other quantum dots or metal nanoclusters. This increased the complexity, cost, and toxicity of nanoprobes [4, 11–13]. Second, some nanoprobes exhibited poor selectivity towards Zn^{2+} owing to the strong interferences of other metal ions (such as Fe^{3+}, Al^{3+}, Cu^{2+}, Ni^{2+}, Pb^{2+}, and Hg^{2+}) [14–19]. Third, most of the nanoprobes were based on single-signal changes. They were susceptible to disturbance from stability of instrument, background noise, and CD concentration. The CD-based fluorescent nanoprobes for ATP also possess the above drawbacks [21–24]. The ratiometric fluorescent nanoprobe is based on the variations of the ratio of fluorescence intensities at two well-resolved emission peaks. They effectively eliminate the external interferences and hence show the outstanding sensitivity and selectivity. The key of the ratio-metric fluorescent nanoprobe is always the design and preparation of dual-emission fluorescent system [25–27]. Considering the particularly complexity of the dual-emission system, the CD-based ratio-metric fluorescent nanoprobes toward Zn^{2+} or ATP were bare [20, 24]. This kind of fluorescent nanoprobe for simultaneously determining Zn^{2+} and ATP has not appeared yet.

The quercetin (QCT) is a flavones present in nature with anticancer, antiviral, anti-mutagenic, and lipid per-oxidation functions [28, 29]. It can form the QCT-Zn^{2+} complex with Zn^{2+} (molar ratio = 1:2) by coordination interactions and emit green fluorescence [18]. The QCT alone can be used as single-signal fluorescent probe for Zn^{2+}. This probe possesses poor stability, limited selectivity, and general sensitivity. As shown in Scheme 1, the red-emission CDs were synthesized and used to construct the ratio-metric fluorescent nanoprobes toward Zn^{2+} and ATP with the aid of QCT. The composition of this probe is simple and eco-friendly. This probe improves the stability, selectivity, and sensitivity of previous single-signal probes. This probe realizes the simultaneously determination of Zn^{2+} and ATP.

Experimental

Materials

QCT, p-phenylenediamine, ATP, adenosine diphosphate (ADP), and mono-phosphate (AMP) were purchased from Shanghai Aladdin Bio-Chem Technology Co, Ltd. (Shanghai, China, http://aladdin-e.bioon.com.cn/). The analytical reagents including NaCl, NaF, NaNO2, NaBr, NaAc, KI, Na2CO3, Na3PO4, NaNO3, Na2HPO4, Na2SO4, Na2S2O3, H2HgN2O7, BaCl2, AlCl3, FeCl3, CuCl2, ZnCl2, CrCl2, CdCl2, MnCl2, Pb(NO3)2, AgNO3, NiCl2, CoCl2, toluene, and ethanol were purchased from Chengdu Kelong Chemical Regent Co, Ltd. (Chengdu, China, http://www.chronchem.com/cn/). All chemicals were used as received without further purification. Ultrapure water was always used throughout the experimental process.

Apparatus

Transmission electron microscopy (TEM) images were recorded on a TEM system (FEI Tecnai G20) operating at 200 kV. The specimen was prepared by drop-casting CD suspension (0.02 mg·mL^{-1}) in ethanol onto a carbon-coated copper grid, followed by drying at room temperature. The X-ray diffraction (XRD) pattern was obtained on an X-ray diffract-meter (X Pert PRO MPD) with a wavelength (λ) of 0.15418 nm. Fourier transform infrared (FTIR) spectra were gained on a FTIR spectrophotometer (WQF-520) by the KBr pellet method. The X-ray photoelectron spectroscopy (XPS) was outperformed on an X-ray photoelectron spectrometer (ESCALAB 250) with a mono-achromatized Al Ka X-ray source (1486.71 eV). UV-visible absorbance and the photoluminescence (PL) spectra were recorded on a UV-visible spectrophotometer (U-4100) and a spectrofluorometer (LS-55), respectively.

Synthesis of red-emission CDs

The red-emission CDs were synthesized according to the reported method with a few modifications [30]. The specific synthesis procedures were described in the Electronic Supplementary Material.

Fluorescent determination of Zn^{2+} and ATP

For determining Zn^{2+}, 1 mL of Zn^{2+} aqueous solutions with different concentrations (0–150 μM) and quantitative F^- (300 μM) were mixed with 1 mL of CD suspensions (0.06 mg·mL^{-1}) and 1 mL of QCT solutions (300 μM) in ethanol under gentle shaking. After 5 min, the fluorescence spectra of above mixtures were taken.

For determining ATP, 1 mL of ATP aqueous solutions with different concentrations (0–150 μM) and quantitative F^- (300 μM) and Zn^{2+} (150 μM) were mixed with 1 mL of CD suspensions (0.06 mg·mL^{-1}) and 1 mL of QCT solutions (300 μM) in ethanol under gentle shaking. After 5 min, the fluorescence spectra of above mixtures were taken.

Results and discussion

Characterization of CDs

The TEM image in Fig. 1 a shows that the nearly spherical CDs were successfully synthesized. These CDs have a narrow particle size distribution of 5.2 ± 2.5 nm. The high-resolution TEM image (Fig. 1b) reflects that the CDs are almost amorphous because no obvious lattice structures can be found. This is consistent with the result of XRD pattern (Fig. S1a). There is only a broad and short peak at 21.7° representing (002) lattice plane of graphite in XRD pattern. This feature further confirms the poor degree of crystalline of CDs.

The FTIR spectrum (Fig. S1b) can reveal the surface groups of CDs. The absorption bands at 3313 and 3198 cm^{-1} can be attributed to the stretching vibrations of O–H and N–H. The bands at 1615 and 1510 cm^{-1} can be owing to the stretching vibrations of C=C, C=N, and C=O. The bands at 1386, 1115, and 833 cm^{-1} can be owing to the deformation vibrations of O–H, stretching vibrations of C–O and C–N, and deformation vibrations of C–H, respectively.

To further probe the surface information of CDs, the XPS data of CDs were gained and shown in Fig. S2. The full-scan XPS spectrum in Fig. S2a shows that the CDs are mainly composed of C, N, and O elements. The C1s XPS spectrum (Fig. S2b) can be deconvoluted into three peaks belonging to the C–C/C=C (284.6 eV), C–O/C–N (285.4 eV), and C=O (287.3 eV) species. The N1s XPS band (Fig. S2c) displays that three N species including pyridine N (398.4 eV), pyrrole N (400.2 eV), and amino N (399.1 eV) can be found. The O1s
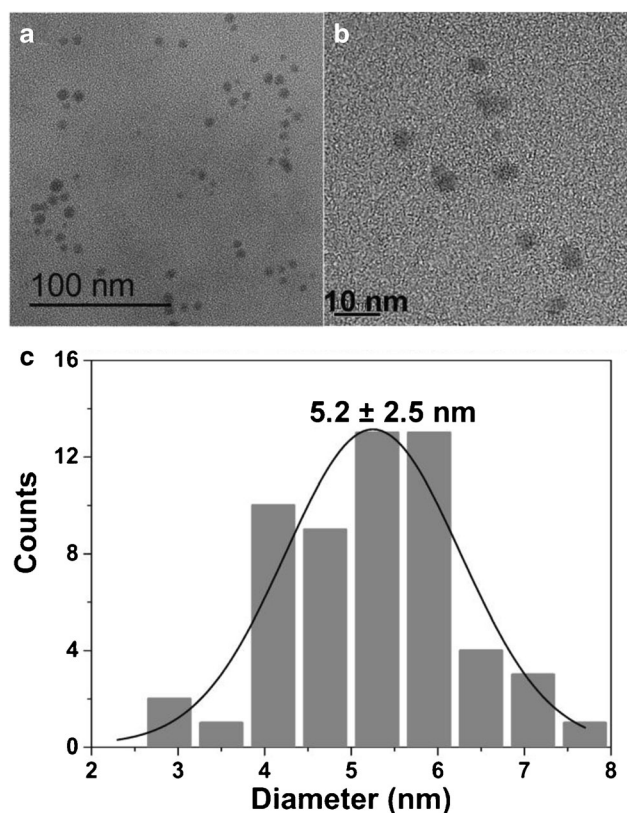

Fig. 1 **a** The TEM, **b** high-resolution TEM images, and **c** the particle size distribution of CDs by counting more than 50 particles

XPS band (Fig. S3d) shows the O elements are composed of C=O (531.4 eV) and C–O–C/C–OH (533.0 eV) species. The results of FTIR and XPS characterization corporately reflect the synthesized CDs which are decorated by amino groups and some oxygen-containing groups. Some N-heterocyclic motifs including pyridine and pyrrole rings also exist in CDs.

Optical properties of CDs

The UV-visible absorption spectrum of CD suspension (Fig. 2a) illustrates a strong absorption peak at 288 nm and a negligible shoulder peak at 325 nm. These can be assigned to the π-π* electronic transitions of aromatic C=C bonds and n-π* transitions of C=N and C=O bonds [31]. An additional prominent shoulder peak between 400 and 600 nm is attributed to the electronic transitions of surface groups and N-heterocyclic motifs [32–34]. The CD suspension has obvious photoluminescence (PL) phenomenon, and the maximum PL excitation and emission wavelengths are at 500 and 610 nm. Figure 2b displays the excitation-independent PL behavior of CDs. The emission wavelength is invariable when the excitation wavelength changes from 300 to 540 nm. This PL behavior reflects that the CDs are uniform not only in particle size but also in surface state. Using quinine sulfate as a reference, the quantum yield of CDs is 18.2% under the excitation

Fig. 2 **a** The UV-visible absorption, maximum PL excitation, and emission spectra of the CD suspension (0.02 mg·mL^{-1}) in ethanol; **b** PL spectra of the CD suspension (0.02 mg·mL^{-1}) recorded at various excitation wavelengths from 320 to 540 nm; Inset of **b**: photos of CD suspension under room light and UV light (365 nm)
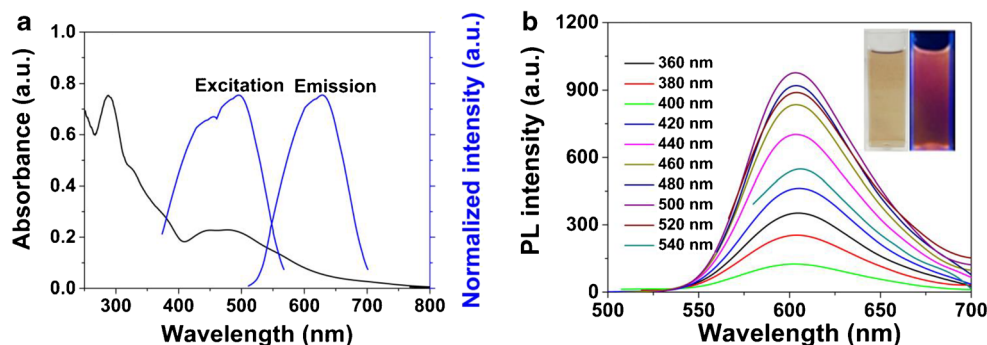
wavelength of 440 nm for determining the Zn^{2+} and ATP (Fig. S3). The CD suspension appears light brown in room light but bright red under the irradiation of UV light (365 nm) (inset in Fig. 2b). This phenomenon further confirms the red-emission feature of CDs. The PL intensity of CD suspension is related to its concentration (c). As shown in Fig. S4a-b, the CDs emit the strongest fluorescence at c of 0.02 mg·mL^{-1}. The PL intensity will reduce because of the self-quenching effect when the c is higher. The pH value also influences the PL intensity of CDs by altering the surface state of CDs. Fig. S4c illustrates that the PL intensity of CDs is strong and stable at a wide pH range of 5.0–11.0. This is beneficial for the fluorescence sensing in aqueous environment. The salt tolerance of CDs is high. That is the PL intensity of CDs is almost constant with increasing c_{NaCl} up to 4 M (Fig. S4d). This is also favorable for fluorescence sensing.

Principle of CD-QCT system as Zn^{2+} ratio-metric fluorescent nanoprobe

As shown in Fig. 3a, QCT (100 μM) alone causes little effect on the PL spectra of CD suspension, while the PL intensity of CD-QCT system (at 610 nm) is greatly quenched when specific amount of Zn^{2+} (50 μM) is further introduced. A new PL peak at 480 nm appears because of the forming QCT-Zn^{2+} complex [18]. Then the CD-QCT system can be constructed as the Zn^{2+} ratio-metric fluorescent nanoprobe on account of the PL intensity ratio (I$_{480}$/I$_{610}$) varying with $c_{Zn}{}^{2+}$. For QCT and Zn^{2+}, each of them can hardly absorb light with wavelength longer than 300 nm. The QCT-Zn^{2+} complex possess

strong absorption at 430 nm. As shown in Fig. 3b, the PL excitation spectrum (440 nm) of CDs is mostly overlapped by the absorption spectrum of QCT-Zn^{2+} complex. Thus, the principle of above Zn^{2+} nanoprobe is confirmed as the inner-filter effect.

Performance of Zn^{2+} ratio-metric fluorescent nanoprobe

The selectivity of CD (0.02 mg·mL^{-1})-QCT (100 μM) system for various metal ions was evaluated and shown in Fig. 4a in terms of the I$_{480}$/I$_{610}$ value. The I$_{480}$/I$_{610}$ values of Zn^{2+} and Al^{3+} systems are much larger than that of blank system and systems containing other metal ions. This result reflects the specific selectivity of CD-QCT system for Zn^{2+} and Al^{3+}. The existence of Al^{3+} will seriously interfere fluorescent sensing of Zn^{2+} owing to the formation of QCT-Al^{3+} complex [35]. To eliminate this possible interference, the F$^-$ ions were introduced into the CD-QCT system as masking regent. As shown in Fig. 4b, the CD (0.02 mg·mL^{-1})-QCT (100 μM)-F$^-$ (100 μM) system exhibits excellent selectivity toward Zn^{2+} and hence can be established as the ratio-metric fluorescent nanoprobe of Zn^{2+}.

The PL spectra and corresponding I$_{480}$/I$_{610}$ values of CD-QCT-F$^-$ systems with different $c_{Zn}{}^{2+}$ were obtained and shown in the Fig. 5. The PL peak at 480 and 610 nm (Fig. 5a) gradually enhances and weakens, respectively, with increasing $c_{Zn}{}^{2+}$. Correspondingly, the I$_{480}$/I$_{610}$ value in Fig. 5b increases little by little. Based on the data in Fig. 5b, the fitted linear relationship between the I$_{480}$/I$_{610}$ value and

Fig. 3 **a** The PL spectra of CD suspension (0.02 mg·mL^{-1}), QCT solution (100 μM), and solution with 100 μM QCT and 50 μM Zn^{2+} under 440 nm irradiation; **b** UV-visible absorption spectrum of solution with 100 μM QCT and 50 μM Zn^{2+} and PL excitation spectrum (440 nm) of CD suspension (0.02 mg·mL^{-1})
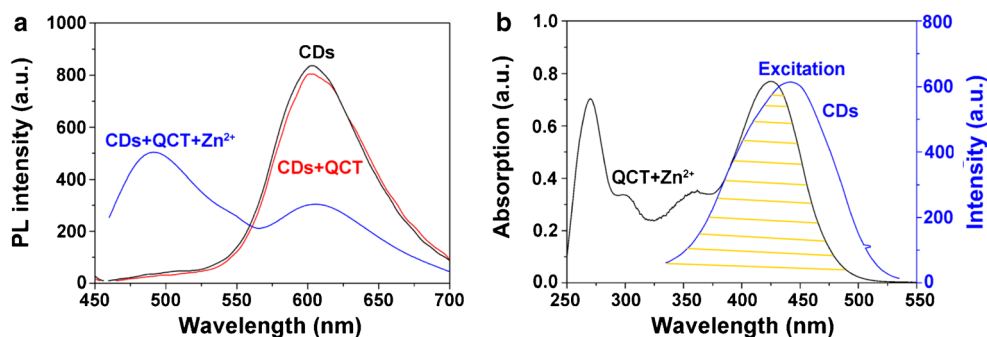
Fig. 4 The selectivity of **a** CD (0.02 mg·mL^{-1})-QCT (100 μM) system and **b** CD (0.02 mg·mL^{-1})-QCT (100 μM)-F$^-$ (100 μM) system toward different metal ions (15 μM) based on the I_{480}/I_{610} value
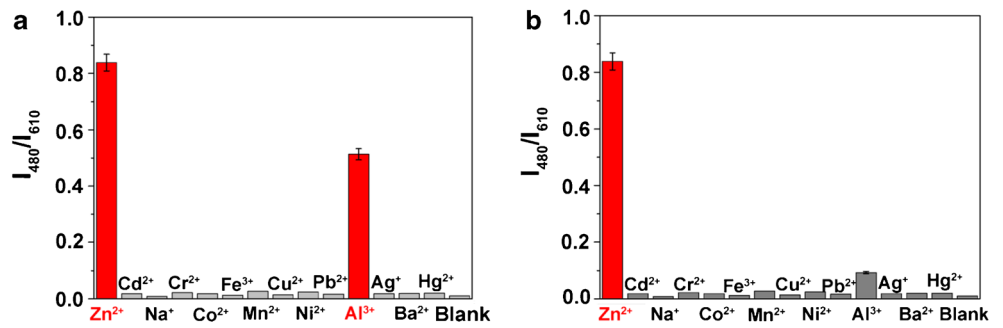

Fig. 5 **a** The PL spectrum and **b** corresponding I_{480}/I_{610} value of CD (0.02 mg·mL^{-1})-QCT (100 μM)-F$^-$ (100 μM) system as a function of $c_{Zn^{2+}}$; Inset of **b**: fitted linear relationship between I_{480}/I_{610} value and $c_{Zn^{2+}}$ (each data point is calculated as the averaged value of 3 repeated experiment)

Inset: $I_{480}/I_{610} = 0.042 c_{Zn^{2+}} + 0.1$
$R^2 = 0.995$

Fig. 6 **a** The PL spectrum and **b** corresponding I_{480}/I_{610} value of CD (0.02 mg·mL^{-1})-QCT (100 μM)-F$^-$ (100 μM)-Zn^{2+} (50 μM) system as a function of c_{ATP}, **c** and **d** Fitted linear relationships between I_{480}/I_{610} value and c_{ATP} (each data point is calculated as the averaged value of 3 repeated experiment)
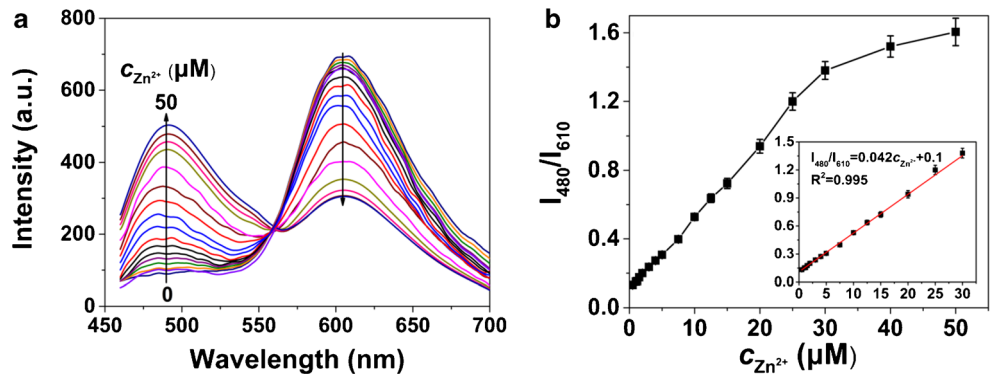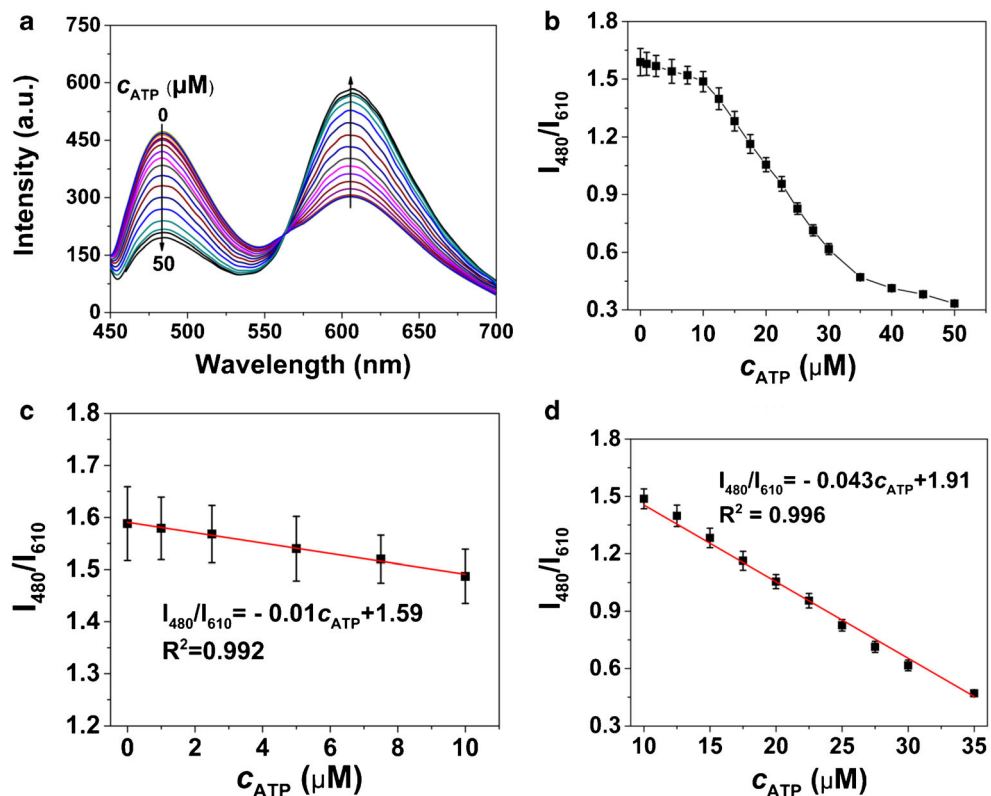

c $I_{480}/I_{610} = -0.01 c_{ATP} + 1.59$
$R^2 = 0.992$

d $I_{480}/I_{610} = -0.043 c_{ATP} + 1.91$
$R^2 = 0.996$

Table 1 An overview on recently reported CD-based fluorescent determination of Zn^{2+} and ATP

Material	Substance	Method	Detection range, LOD (μM)	Interference	Reference
Quinoline derivative-capped CDs	Zn^{2+}	Fluorescence	0.1–2.0 μM, 6.4 nM	Cu^{2+}, Cd^{2+}	[11]
CD-QCT	Zn^{2+}	Fluorescence	2–200 μM, 2 μM	Al^{3+}	[18]
CDs	Zn^{2+}	Fluorescence	Unattained, >1 μM	Many metal ions	[14]
P-doped CDs	Zn^{2+}	Fluorescence	1–11 μM, 0.4 μM	Many metal ions	[15]
CD-Au cluster	Zn^{2+}	Ratio-metric Fluorescence	1–70 μM, 0.1 μM	–	[12]
Cylix[4]arena-modified CDs	Zn^{2+}	Fluorescence	1–20 μM, 7.34 nM	–	[4]
CdTe dot-CD	Zn^{2+}	Ratio-metric Fluorescence	0.5–40 μM, 0.33 μM	–	[13]
Zn-doped CD-EDTA	Zn^{2+}	Fluorescence	2–15 μM, 0.51 μM	–	[16]
CD-HClO	Zn^{2+}	Fluorescence	8.4–84 μM, 0.3 μM	Cu^{2+}, Fe^{3+}	[19]
Dual-emission CDs	Zn^{2+}	Ratio-metric Fluorescence	2.5–50 μM, 1.2 μM	–	[20]
Red-emission CD-QCT-F^-	Zn^{2+}	Ratio-metric Fluorescence	0.14–30 μM, 0.14 μM	–	This work
CD-metal ion ensembles	ATP	Fluorescence	0.5–6 μM, 0.11 μM	–	[21]
CD-Fe^{3+}	ATP	Fluorescence	0.1–450 μM, 5 nM	–	[22]
CD-Au nanorod	ATP	Ratio-metric Fluorescence	0–50 μM, 3.6 μM	–	[23]
CD-calcein-Eu^{3+}	ATP	Ratio-metric Fluorescence	0.05–2 μM, 20 nM	–	[24]
Red-emission CD-QCT-F^--Zn^{2+}	ATP	Ratio-metric Fluorescence	0.55–35 μM, 0.55 μM	–	This work

Table 2 Recovery tests of Zn^{2+} and ATP in spiked tap and lake water samples analyzed by the above two ratio-metric fluorescent nanoprobes

Sample	Substance	Added (μM)	Found (μM)	Recovery (%)	RSD ($n = 3$, %)
Tap water	Zn^{2+}	0.0	0.23	-	3.2
		6.0	6.05	97.1	4.6
		12.0	11.9	97.3	2.9
	ATP	8.0	8.14	102	2.7
		24.0	23.4	97.7	3.1
Lake water	Zn^{2+}	0.0	0.41	-	3.4
		6.0	6.23	97.0	2.9
		12.0	12.9	104	3.8
	ATP	8.0	7.84	98.0	3.3
		24.0	22.9	95.4	4.0

c_{Zn}^{2+} with high degree of fitting ($R^2 = 0.995$) is obtained (Inset of Fig. 5b). The detection range of this probe is confirmed as 0.14–30 μM. According to the 3σ IUPAC criteria, the limit of detection (LOD) of this probe is calculated as 0.14 μM.

The selectivity of above Zn^{2+} nanoprobe was further evaluated. There are a lot of inorganic ions (such as K^+, Ca^{2+}, Mg^{2+}, Fe^{3+}, F^-, Cl^-, SO_4^{2-}) in tap water. Fig. S5 displays that the CD-QCT-F^- system can still be used as the ratio-metric fluorescent nanoprobe of Zn^{2+} when the ultrapure water of test systems was displaced by the tap water. The probe has similar linear detection range of 0.15–30 μM and LOD of 0.15 μM.

Principle and performance of ATP ratio-metric fluorescent nanoprobe

The UV-visible absorption spectra of various solutions shown in Fig. S6a demonstrate the feature absorption peak of QCT-Zn^{2+} complex at 430 nm disappear when the ATP is introduced. The typical absorption peaks for QCT at 382 nm and for ATP at 267 nm appear. These phenomena indicate that the affinity of ATP to Zn^{2+} is much stronger than QCT. Addition of ATP into the CD-QCT-F^--Zn^{2+} system can result in the decomposition of QCT-Zn^{2+} complex. This makes the green fluorescence at 480 nm attenuate under 440 nm irradiation. The red fluorescence of CDs at 610 nm recovers. Then the CD-QCT-F^--Zn^{2+} system can be builted as a ratio-metric fluorescent nanoprobe of ATP based on the I_{480}/I_{610} value varying with c_{ATP}.

Fig. S6b displays the selectivity of CD-QCT-F^--Zn^{2+} system toward different analytic substances. Not only common inorganic anions but also analogues of ATP (such as AMP and ADP) can hardly interfere the fluorescent sensing of ATP. This confirms the specific selectivity of CD-QCT-F^--Zn^{2+} system toward ATP.

As shown in Fig. 6, the PL peak at 480 and 610 nm gradually weakens and enhances, respectively, with increasing c_{ATP}. Correspondingly, the I_{480}/I_{610} value in Fig. 6b reduces little by little. Two fitted linear relationships between I_{480}/I_{610} value and c_{ATP} with high degree of fitting ($R^2 > 0.99$) are gained as 0.55–10 (Fig. 6c) and 10–35 μM (Fig. 6d). Then the ratio-metric fluorescent nanoprobe of ATP is built with LOD of 0.55 μM and determination ranges of 0–10 μM and 10–35 μM. This nanoprobe has comparable sensitivity and favorable determination range but much better selectivity compared with the previous CD-based fluorescent nanoprobes of ATP [21–24].

Table 1 lists the performances of the recently reported and the above CD-based fluorescent probes towards Zn^{2+} and ATP. Some previous probes have complicated or toxic or expensive compositions. The compositions of our probes are simple, cheap, and eco-friendly. Most of the previous probes are based on single-signal changes. These probes usually show relatively poor sensitivity and selectivity. Our probes

are on account of the ratio-metric fluorescence variations with favorable sensitivity and selectivity. Previous probes can determine either Zn^{2+} or ATP. Our probes realize simultaneously determination of Zn^{2+} and ATP. Some drawbacks are also existent in our probes. The CDs and QCT possess the poor water-solubility and hence perplex the determination procedures of Zn^{2+} and ATP. This method may not be used in vivo because the Zn^{2+} and ATP are coexisting.

Recovery tests in tap and lake water samples

To evaluate the reliability of the above two nanoprobes, the recovery tests of Zn^{2+} and ATP in spiked tap and lake water samples were carried out. The lake water was directly obtained from the college of Southwest Petroleum University (Chengdu, China). It was used after filtering through a membrane (0.22 μm) and centrifuging at 12,000 r min^{-1} for 10 min. The recoveries of spiked samples shown in Table 2 all range between 95 and 104% with low relative standard deviation (RSD). The satisfactory recovery results mean that the ratio-metric fluorescent nanoprobes presented here can realize the quantitative determination of Zn^{2+} and ATP in real samples.

Conclusions

The red-emission CD-QCT-F system was constructed as the ratio-metric fluorescence probe of Zn^{2+} based on the inner filter effect of the QCT-Zn^{2+} complex. The detection range and LOD of this probe are 0.14–30 μM and 0.14 μM. The CD-QCT-F^--Zn^{2+} system was built as the ratio-metric fluorescent probe of ATP with detection ranges of 0.55–10 and 10–35 μM and LOD of 0.55 μM. These probes are composed of simple and eco-friendly materials. The sensitivity and selectivity of these probes are satisfactory. The probes presented here realize simultaneously determination of Zn^{2+} and ATP in tap and lake water samples. There are also two striking drawbacks for the above two probes. The CDs and QCT are poorly soluble in water and hence perplex the determination procedures of Zn^{2+} and ATP. This method cannot be used in vivo because the Zn^{2+} and ATP are coexisting.

Compliance with ethical standards

Conflict of interest The authors declare that they have no conflict of interests.

References

1. Berg JM, Shi Y (1996) The galvanization of biology: a growing appreciation for the roles of zinc. Science 271:1081–1085

2. Beyersmann D, Haase H (2001) Functions of zinc in signaling, proliferation and differentiation of mammalian cells. Biometals 14:331–341

3. Vasto S, Candore G, Listì F, Balistreri CR, Colonna-Romano G, Malavolta M, Lio D, Nuzzo D, Mocchegiani E, Di Bona D, Caruso C (2008) Inflammation, genes and zinc in Alzheimer's disease. Brain Res Rev 58:96–105

4. Kaur H, Raj P, Sharma H, Verma M, Singh N, Kaur N (2018) Highly selective and sensitive fluorescence sensing of nanomolar Zn^{2+} ions in aqueous medium using calix 4 arene passivated carbon quantum dots based on fluorescence enhancement: real-time monitoring and intracellular investigation. Anal Chim Acta 1009:1–11

5. Zhou Q, Lin Y, Lin Y, Wei Q, Chen G, Tang D (2016) In situ amplified electrochemical aptasensing for sensitive detection of adenosine triphosphate by coupling target-induced hybridization chain reaction with the assembly of silver nanotags. Talanta 146: 23–28

6. Li X, Peng Y, Chai Y, Yuan R, Xiang Y (2016) A target responsive aptamer machine for label-free and sensitive non-enzymatic recycling amplification detection of ATP. Chem Commun 52: 3673–3676

7. Dong YQ, Wang RX, Li GL, Chen CQ, Chi YW, Chen GN (2012) Polyamine-functionalized carbon quantum dots as fluorescent probes for selective and sensitive detection of copper ions. Anal Chem 84:6220–6224

8. Wang B, Ln Y, Tan H, Luo M, Dai S, Lu H, Huang Z (2018) One-pot synthesis of N-doped carbon dots by pyrolyzing the gel composed of ethanolamine and 1-carboxyethyl-3-methylimidazolium chloride and their selective fluorescence sensing for Cr(VI) ions. Analyst 143:1906–1915

9. Wang B, Tan H, Zhang T, Duan W, Zhu Y (2019) Hydrothermal synthesis of N-doped carbon dots from an ethanolamine-ionic liquid gel to construct label-free multifunctional fluorescent probes for Hg^{2+}, Cu^{2+} and $S_2O_3^{2-}$. Analyst 144:3013–3022

10. Zu FL, Yan FY, Bai ZJ, Xu JX, Wang YY, Huang YC, Zhou XG (2017) The quenching of the fluorescence of carbon dots: a review on mechanisms and applications. Microchim Acta 184:1899–1914

11. Zhang Z, Shi Y, Pan Y, Cheng X, Zhang L, Chen J, Li MJ, Yi C (2014) Quinoline derivative-functionalized carbon dots as a fluorescent nanosensor for sensing and intracellular imaging of Zn^{2+}. J Mater Chem B 2:5020–5027

12. Han B, Peng T, Yu M, Chi C, Li Y, Hu X, He G (2018) One-pot synthesis of highly fluorescent Fe^{2+}-doped carbon dots for a dual-emissive nanohybrid for the detection of zinc ions and histidine. New J Chem 42:13651–13659

13. Song Q, Ma Y, Wang X, Tang T, Song Y, Ma Y, Xu G, Wei F, Cen Y, Hu Q (2018) "on-off-on" fluorescent system for detection of Zn^{2+} in biological samples using quantum dots-carbon dots ratiometric nanosensor. J Colloid Interface Sci 516:522–528

14. Kumar VV, Raman T, Anthony SP (2017) Fluorescent carbon quantum dots chemosensor for selective turn-on sensing of Zn^{2+} and turn-off sensing of Pb^{2+} in aqueous medium and zebrafish eggs. New J Chem 41:15157–15164

15. Omer KM, Hassan AQ (2017) Chelation-enhanced fluorescence of phosphorus doped carbon nanodots for multi-ion detection. Microchim Acta 184:2063–2071

16. Yang M, Tang Q, Meng Y, Liu J, Feng T, Zhao X, Zhu S, Yu W, Yang B (2018) Reversible "off-on" fluorescence of Zn^{2+}-passivated carbon dots: mechanism and potential for the detection of EDTA and Zn^{2+}. Langmuir 34:7767–7775

17. Yu L, Ren G, Tang M, Zhu B, Chai F, Li G, Xu D (2018) Effective determination of Zn^{2+}, Mn^{2+}, and Cu^{2+} simultaneously by using dual-emissive carbon dots as colorimetric fluorescent probe. Eur J Inorg Chem 29:3418–3426

18. Yang M, Kong W, Li H, Liu J, Huang H, Liu Y, Kang Z (2015) Fluorescent carbon dots for sensitive determination and intracellular imaging of zinc(II) ion. Microchim Acta 182:2443–2450

19. Zhang Z, Pei K, Yang Q, Dong J, Yan Z, Chen J (2018) A nanosensor made of sulfur-nitrogen co-doped carbon dots for "off-on" sensing of hypochlorous acid and Zn(II) and its bioimaging properties. New J Chem 42:15895–15904

20. Wang Y, Lao S, Ding W, Zhang Z, Liu S (2019) A novel ratiometric fluorescent probe for detection of iron ions and zinc ions based on dual-emission carbon dots. Sensors Actuators B Chem 284:186–192

21. Sun S, Jiang K, Qian S, Wang Y, Lin H (2017) Applying carbon dots-metal ions ensembles as a multichannel fluorescent sensor array: detection and discrimination of phosphate anions. Anal Chem 89:5542–5548

22. Huang Q, Li Q, Chen Y, Tong L, Lin X, Zhu J, Tong Q (2018) High quantum yield nitrogen-doped carbon dots: green synthesis and application as "off-on" fluorescent sensors for the determination of Fe^{3+} and adenosine triphosphate in biological samples. Sensors Actuators B Chem 276:82–88

23. Srinivasan S, Ranganathan V, DeRosa MC, Murari BM (2019) Comparison of turn-on and ratiometric fluorescent G-quadruplex aptasensor approaches for the detection of ATP. Anal Bioanal Chem 411:1319–1330

24. Zhang C, Zhang H, Yu Y, Wu S, Chen F (2019) Ratio fluorometric determination of ATP base on the reversion of fluorescence of calcein quenched by Eu(III) ion using carbon dots as reference. Talanta 197:451–456

25. He Y, Yu Z, He J, Zhang H, Liu Y, Lei B (2018) Ratiometric and selective fluorescent sensor for Fe(III) and bovine serum albumin based on energy transfer. Sensors Actuators B Chem 262:228–235

26. Liu W, Wang X, Wang Y, Li J, Shen D, Kang Q, Chen L (2018) Ratiometric fluorescence sensor based on dithiothreitol modified carbon dots-gold nanoclusters for the sensitive detection of mercury ions in water samples. Sensors Actuators B Chem 262:810–817

27. Jiao Y, Gao Y, Meng Y, Lu W, Liu Y, Han H, Shuang S, Li L, Dong C (2019) One-step synthesis of label-free ratiometric fluorescence carbon dots for the detection of silver ions and glutathione and cellular imaging applications. ACS Appl Mater Interfaces 11: 16822–16829

28. Hollman PCH, Hertog MGL, Katan MB (1996) Role of dietary flavonoids in protection against cancer and coronary heart disease. Biochem Soc Trans 24:785–789

29. Moreira AJ, Fraga C, Alonso M, Collado PS, Zetller C, Marroni C, Marroni N, González-Gallego J (2004) Quercetin prevents oxidative stress and NF-κB activation in gastric mucosa of portal hypertensive rats. Biochem Pharmacol 68:1939–1946

30. Zhang T, Zhu J, Zhai Y, Wang H, Bai X, Dong B, Wang H, Song H (2017) A novel mechanism for red emission carbon dots: hydrogen bond dominated molecular states emission. Nanoscale 9:13042–13051

31. Li H, Xu Y, Zhao L, Ding J, Chen M, Chen G, Li Y, Din L (2019) Synthesis of tiny carbon dots with high quantum yield using multi-

walled carbon nanotubes as support for selective "turn-off-on" detection of rutin and Al^{3+}. Carbon 143:391–401

32. Zhu S, Song Y, Zhao X, Shao J, Zhang J, Yang B (2015) The photoluminescence mechanism in carbon dots (graphene quantum dots, carbon nanodots, and polymer dots): current state and future perspective. Nano Res 8:355–381

33. Zhu S, Shao J, Song Y, Zhao X, Du J, Wang L, Wang H, Zhang K, Zhang J, Yang B (2015) Investigating the surface state of graphene quantum dots. Nanoscale 7:7927–7933

34. Ding H, Yu SB, Wei JS, Xiong HM (2016) Full-color light-emitting carbon dots with a surface-state-controlled luminescence mechanism. ACS Nano 10:484–491

35. Zou Y, Yan F, Dai L, Luo Y, Fu Y, Yang N, Wun J, Chen L (2014) High photoluminescent carbon nanodots and quercetin-Al^{3+} construct a ratiometric fluorescent sensing system. Carbon 77:1148–1156